Acta Materialia 103 (2016) 461–473

Contents lists available at ScienceDirect

Acta Materialia

journal homepage: www.elsevier.com/locate/actamat

A combined grain scale elastic–plastic criterion for identification of fatigue crack initiation sites in a twin containing polycrystalline nickel-base superalloy

J.C. Stinville [a,*], W.C. Lenthe [a], J. Miao [b], T.M. Pollock [a]

[a] Materials Department, University of California Santa Barbara, Santa Barbara, CA, USA
[b] Department of Material Science and Engineering, University of Michigan, Ann Arbor, MI, USA

ARTICLE INFO

Article history:
Received 2 July 2015
Received in revised form 2 September 2015
Accepted 25 September 2015
Available online 6 November 2015

Keywords:
René 88DT superalloy
Coherent twin boundary
Very high cycle fatigue
Low cycle fatigue
Elastic anisotropy
Schmid factor

ABSTRACT

Damage initiation during cycling loading of polycrystalline metallic alloys involves localized damage at the scale of individual grains. To better understand damage processes and to build models for material behavior, there is a need for quantitative assessment of the microstructural configurations that favor fatigue crack initiation. In materials that form annealing twins during processing, these special interfaces are often locations of particular interest for their role in strain and damage accumulation. In the present study, fatigue experiments in the very high and low cycle fatigue regime on a René 88DT polycrystalline nickel-base superalloy were performed to statistically evaluate grain-scale features that favor crack initiation. Combined elastic and plastic criteria at the grain scale have been developed. A crack distribution function is defined to compare and assess the effect of the microstructural parameters for the two fatigue regimes.

1. Introduction

Predicting fatigue crack initiation in polycrystalline engineering materials remains a major challenge due to the inherent sensitivity of the initiation process to the details of the microstructure. Under many realistic loading scenarios, the strain amplitude in fatigue cycling is relatively low, with the implications that (1) initiation consumes a large fraction of the overall cyclic life and (2) both the elastic and plastic properties of the material may strongly influence the initiation process. Furthermore, in materials that form annealing twins during processing (stainless steels and Ni, Cu, Al and Ag alloys), this feature of the microstructure is of special interest for its influence on fatigue damage development. Miao et al. [1,2] reported that cracks initiated in high Schmid factor grains with slip planes parallel to and slightly offset from coherent twin boundaries in the nickel-based alloy René 88DT under very high cycle fatigue loading. Crack initiation during cycling loading has been observed along twin boundaries for various other twin-containing materials including other nickel-base superalloys [1–3], stainless steels [4] and copper [5,6]. Heinz and Neumann [7] first suggested that elastic anisotropy causes a local stress concentration that strongly enhances glide at twin boundaries. For the case of face centered cubic (fcc) coherent twins, the boundaries are always parallel to a slip plane, so dislocations can travel across the entire diameter of a grain, creating a stress concentration, particularly if the slip is localized on a single system. Heinz and Neumann [7] emphasized that these twins lead to stronger strain localization than a general grain boundary with oblique slip planes. Stein, Rollett, Ingraffea et al. [8,9] report very high stresses near twin boundaries when slip occurs parallel to twin boundaries using crystal plasticity models for superalloys. Stinville et al. [10], using subgrain digital image correlation (DIC) measurements at the microscale, report local strain enhancement of a factor of 4–10 near these coherent twin boundaries during straining. A variety of microstructure parameters have been reported to contribute to cyclic strain localization and fatigue crack initiation at twin boundaries. Fatigue cracks have been found to initiate in grains at the high end of the grain size distribution in twin-containing materials during high cycle fatigue [1,2,11–13]. In addition, grains oriented favorably for slip (high resolved shear stress slip systems) are observed to initiate cracks [1,14,15]. Moreover, elastic anisotropy has been shown to induce significant stress heterogeneities from grain to grain [16,17],

* Corresponding author.
E-mail address: stinville@engineering.ucsb.edu (J.C. Stinville).

http://dx.doi.org/10.1016/j.actamat.2015.09.050
1359-6454/

strongly influencing crack initiation, particularly at lower strain amplitudes [7]. Under low deformation amplitudes, Heinz and Neumann [7] have shown that fcc materials exhibiting relatively strong elastic anisotropy experience elevated shear stresses at twin boundaries, which ultimately triggers local plasticity and crack initiation. However, the contribution of each of these material features on the crack initiation process and their interplay remain unclear. A better understanding of the role of microstructural parameters in the development of fatigue damage in twin containing materials is crucial for the prediction of fatigue life and fatigue life variability.

The present study investigates the effects of microstructural configuration on fatigue crack initiation in a twin-containing material at room temperature for loading conditions in the low cycle and very high fatigue regime. Investigation of a large number of cracks initiating near twin boundaries has been performed with consideration of both microstructural and mechanical parameters. A combined elastic–plastic criterion at the grain scale is shown to predict locations of crack initiation near twin boundaries. In addition, a crack distribution function that statistically isolates grains most likely to initiate cracks is defined to compare and assess the effect of the microstructural parameters for the two fatigue regimes.

2. Experimental procedure

2.1. Material

The material tested in this study is the polycrystalline nickel-based superalloy, René 88DT. This production alloy is processed through a powder metallurgy route. The nominal alloy chemistry is: 13%Co, 16%Cr, 4%Mo, 4%W, 2.1%Al, 3.7%Ti, 0.7%Nb, 0.03%C, 0.015%B (weight percent) [18,19]. The microstructure of the alloy consists of a γ matrix and two populations of spherical gamma prime (γ') precipitates; including larger secondary γ' (≈100–200 nm in diameter) and nm-scale tertiary γ' (several nanometers in diameter). Due to the super-solvus nature of the solution anneal, the microstructure of René 88DT contains no sub-solvus γ', which is usually termed primary [19]. The material possesses very weak crystallographic texture, a large population of $\Sigma3$ grain boundaries (58% of the total boundary fraction), and an average grain size of 26 µm. Crystallographic features have been previously detailed (see Ref. [20]) using electron backscatter diffraction (EBSD) measurements.

2.2. Mechanical tests

Cyclic testing was performed in air at room temperature in the low cycle fatigue and very high cycle fatigue regimes. Low cycle fatigue tests were performed in a symmetric, uniaxial, push–pull mode on an electromechanical machine. Tests were carried out in stress control mode at maximum stress of 758 MPa, with a R-ratios of –1 and 0.1 and a frequency of 1 Hz. Cylindrical specimens with a gauge diameter of 5 mm and gauge length of 16 mm were used in this study. Strain was measured by a mechanical extensometer positioned on the gauge. Interrupted tests were performed to enable crack density, crack size and sub-grain DIC measurements at different percentages of the lifetime. Very high cycle fatigue testing was conducted under fully reversed loading (R-ratio of –1) using an ultrasonic fatigue instrument [36–40] operating at a frequency close to 20 kHz. Details of the ultrasonic fatigue testing technique can be found in Ref. [11]. Cylindrical ultrasonic fatigue specimens with a gauge diameter of 5 mm and a gauge length of 18 mm were used. After fatigue testing, specimen surfaces were examined using scanning electron microscopy to identify regions exhibiting evidence of microcrack formation.

2.3. Sample preparation for EBSD, crack density and crack size measurements

EBSD measurements require the use of flat specimens. Therefore two flat areas, 2.5 mm in width and 8 mm in length, were machined on the gauge of selected fatigue specimens. The two flats were positioned on opposite sides of the specimen in the gauge section. Moreover, in order to obtain high quality back-scattered electron diffraction patterns, it was essential to remove any residual stresses in the surface layer due to sample preparation. This required removing a thin surface layer by electropolishing the samples in a solution of 10% of perchloric acid and 90% of ethylene glycol at 30 V. Finally, the gauge length of some specimens was etched with a Fe (III) chloride + HCL solution in order to produce a nm-scale speckle pattern which is favorable for sub-grain scanning electron microscopy digital image correlation (SEM-DIC) without interfering with EBSD measurements [21].

Crack density measurements were made on two flat surfaces with an investigated surface area of 2.5×8 mm^2 on each side of the specimen. Surface crack sizes were determined using secondary electron imaging and measuring the length of the entire path of the crack.

The geometry of the flat areas was designed to limit the potential stress concentration induced by the presence of edges produced during machining of the flat areas. In addition, careful mechanical polishing was performed to further reduce any local concentrations. This process resulted in crack densities and lifetimes that were indistinguishable in specimens with and without flat areas.

2.4. Sub-grain scanning electron microscopy digital image correlation

In-plane displacement fields at the microscopic scale were obtained using DIC open source software (OpenDIC) [22]. SEM (secondary electron microscopy) images (5120×3840 pixels) were divided into custom sized subsets of 27×27 pixels regularly spaced by 17 pixels in both horizontal “X” and vertical “Y” directions. The correlation was based on the zero-normalized cross-correlation (ZNCC) criterion [23]. The correlation of each subset is fully independent from the correlation of neighboring subsets. Deformed images were interpolated by a factor 10 using a biquintic polynomial interpolation algorithm. The interpolation led to a theoretical resolution of 0.1 pixel (~6.2 nm at ×1000 magnification) for the displacements within each subset. A companion application was implemented in MatLab to calculate and plot the in-plane strain fields (ε_{xx}, ε_{yy} and ε_{xy}) at each point of the image from the displacement fields, U_X and U_Y, in the X (loading) direction and Y direction, respectively. The strain calculation was based on the isoparametric 2D finite element formalism using subset centers as nodes and introducing four Gauss bilinear interpolation points per element. Direct DIC measurements (cumulative) have been chosen, so the direct strain map is obtained by comparing after each deformation step the micrograph of the deformed specimen with the micrograph of the undeformed specimen. Details of the sub-grain SEM-DIC technique can be found in Ref. [17] and in Ref. [10].

3. Results

3.1. Low cycle fatigue regime

A total of 10 cyclic deformation tests were performed on cylindrical specimens in air under load control conditions at maximum stress of 758 MPa with a R-ratio of –1 and a frequency of 1 Hz at room temperature. The average lifetime of these specimens was 65340 cycles with a scatter (standard deviation) of 5530 cycles. A maximum and minimum total strain of 0.35% ± 0.04% and –0.35% ± 0.03% was measured for the first cycle. The material exhibited cyclic evolution of the strain with the maximum and minimum strain stabilizing at 0.40% ± 0.05% and –0.30% ± 0.04% respectively after half of the lifetime. The strain range remained constant (0.70% ± 0.03%) during the entire fatigue test.

Fracture surfaces of all failed fatigue samples were examined using SEM and surface initiation was observed for all failed specimens. Fatigue cracks initiated in microstructural regions consisting of large crystallographic facets (Fig. 1). Interrupted fatigue tests were conducted to assess the microstructure associated with initiation sites. Multiple cracks at the surface of the fatigue specimens within individual grains were observed during cycling. Fig. 1 presents the fatal crack after 32% (Fig. 1a) and 81% (Fig. 1b) of the lifetime associated with the initiation site observed on the fracture surface in Fig. 1d. Fig. 1c shows the inverse pole figure map along the loading direction associated with Fig. 1a. Using crystallographic information measured by EBSD, the Schmid factors for all 12 {1 1 1} < 1 1 0 > octahedral face-centered cubic (fcc) slip systems in both the twin and parent grain were calculated and are shown in Table 1. All investigated cracks (more than 50 secondary and fatal cracks) initiated near a Σ3 twin boundary. In addition, the slip systems with the highest resolved shear stress in both the twin and parent grain associated with the initiation site have their plane trace (Fig. 1c) parallel to the twin boundary, i.e. the twin and associated parent grain exhibit a parallel slip configuration (see Ref. [10]).

Fig. 2 presents a secondary crack initiation site after 45% of the lifetime. Interestingly, significant extrusion of material is observed at the initiation site. Extrusion to a greater or lesser extent was observed for all investigated cracks.

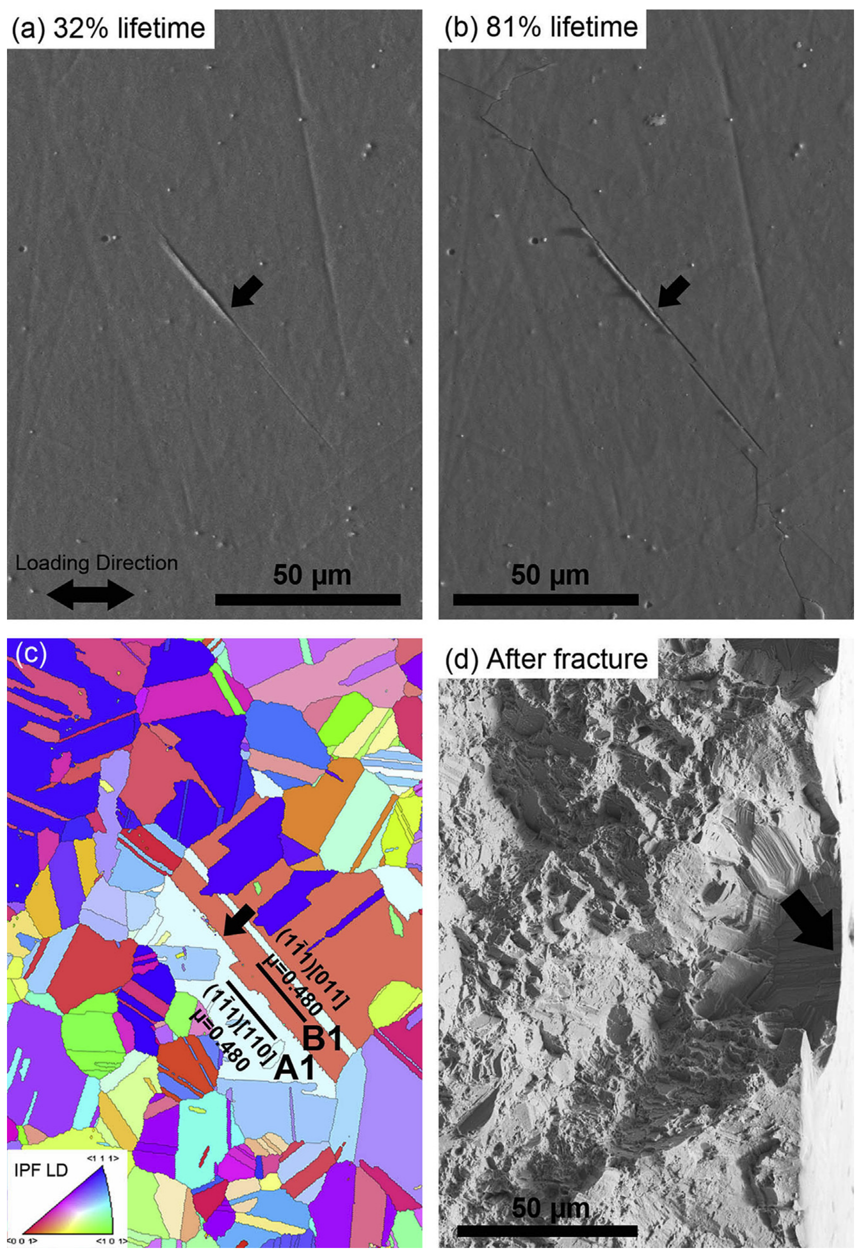

Fig. 1. Microstructural and damage features of the initiation site: (a) surface of a fatigue sample after 32% of the fatigue lifetime showing the fatal crack, (b) fatal crack after 81% of the fatigue lifetime, (c) associated inverse pole figure map along the loading direction, (d) fracture surface of the failed sample. Arrows indicate the location of the initiation site.

Table 1
Schmid factor for the 12 fcc slip systems in pairs A1-B1, A2-B2, A3-B3, A4-B4 and A5-B5. Bold values indicate maximum Schmid factors.

Slip system	$(\bar{1}11)$			(111)			$(\bar{1}\bar{1}1)$			$(1\bar{1}1)$		
	$[01\bar{1}]$	$[101]$	$[\bar{1}\bar{1}0]$	$[01\bar{1}]$	$[\bar{1}01]$	$[1\bar{1}0]$	$[0\bar{1}\bar{1}]$	$[101]$	$[\bar{1}10]$	$[0\bar{1}\bar{1}]$	$[\bar{1}01]$	$[110]$
Grain												
A1	0.044	0.010	0.034	0.280	0.154	0.126	0.188	0.200	0.388	0.138	0.341	**0.480**
B1	0.465	0.079	0.387	0.298	0.103	0.401	0.284	0.041	0.325	**0.480**	0.139	0.340
A2	**0.493**	0.212	0.281	0.207	0.038	0.245	0.242	0.139	0.381	0.458	0.112	0.346
B2	0.211	0.282	**0.493**	0.278	0.153	0.431	0.340	0.157	0.187	0.149	0.028	0.120
A3	0.453	0.187	0.266	0.179	0.133	0.311	0.133	0.041	0.174	0.220	0.279	**0.499**
B3	0.223	0.117	0.340	0.475	0.159	0.316	0.199	0.056	0.255	**0.499**	0.220	0.279
A4	0.221	0.044	0.177	0.349	0.135	0.214	0.311	0.149	0.461	0.258	0.240	**0.498**
B4	0.457	0.163	0.294	0.200	0.136	0.336	0.158	0.043	0.201	**0.499**	0.256	0.242
A5	0.418	0.014	0.423	0.389	0.050	**0.437**	0.387	0.011	0.376	0.420	0.042	0.378
B5	0.078	0.022	0.100	**0.438**	0.386	0.052	0.285	0.202	0.084	0.075	0.162	0.236

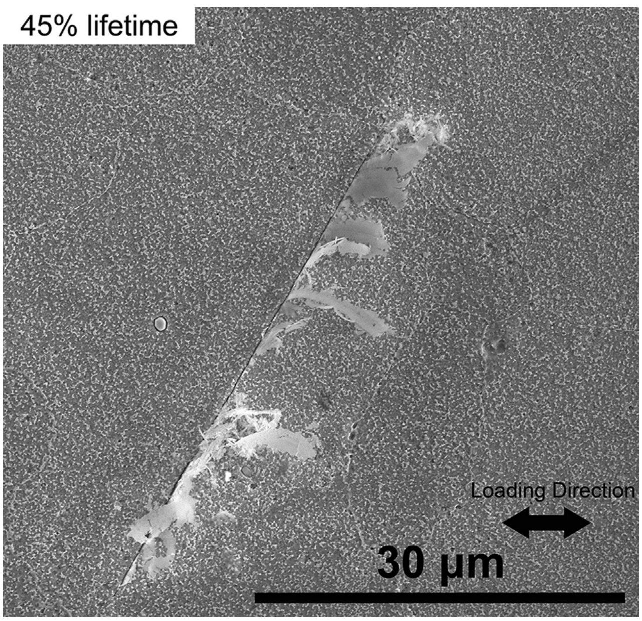

Fig. 2. Damage features of an initiation site near twin boundary: significant extrusion of material from the crack is observed for fatigue cycling at maximum stress of 758 MPa.

3.1.1. *Surface damage evolution*

A total of 50 surface cracks have been classified during cycling according to their length with respect to the microstructure (see Ref. [24]). Type I cracks are confined to one grain. Type II cracks extend between one and three grain diameters, crossing one or two grain boundaries on the surface. Type III cracks have propagated through three to ten surface grains. Type IV surface cracks are longer than ten grain diameters. Specimens typically exhibited only one or two type IV cracks during the final 15% of the fatigue lifetime. Type IV cracks are generally associated with the propagation stage, observed to be primarily governed by mechanics of the growth of long cracks and are not strongly influenced by microstructure. Conversely, microstructural and crystallographic features of the material govern the behavior of Type I, II, and III cracks. The evolution of surface crack density and size over fatigue lifetime is shown in Fig. 3. The different crack types (type I to IV) are reported in the plot. Fig. 3a reports the maximum, the minimum and the average crack size observed in surface during cycling.

Type IV cracks appear after 80% of lifetime and ultimately lead to failure. These cracks are first detected at the individual grain scale after 20% of lifetime i.e. fatigue damage growth dominates 80% of fatigue lifetime. Crack density increases until 80% of fatigue lifetime then decreases slightly due to crack coalescence events. Fig. 4 shows the crack density evolution during cycling according crack type (Fig. 4a) and size (Fig. 4b). Between 30% and 40% of lifetime, cracks are confined in a single grain (type I in Fig. 3a). After 40% of lifetime, some cracks overcome grain boundaries and propagate in neighboring grains. It is worth noting that a significant fraction (about 40%) of cracks do not propagate into neighboring grains, remaining confined in the initiated grain until rupture. Thus, it is apparent that specific microstructural neighborhoods favor crack propagation. After half of the lifetime, cracks transition from type II to type III (Fig. 3a). All cracks that overcome grain boundaries and propagate into neighboring grains, continue to grow during the cycling (Fig. 4b).

3.1.2. *Crack initiation*

3.1.2.1. Local strain accumulation. Fig. 5 shows a region of interest that was imaged during an interrupted fatigue test at maximum stress of 758 MPa. The strain field, ε_{xx} (along the loading direction), is presented for fatigue test interruptions after 1 cycle (Fig. 5a), 15% of the lifetime (Fig. 5b), and 45% of the lifetime (Fig. 5c). The associated EBSD map (before loading) and SEM images after 1 cycle and 45% of the lifetime are reported in Fig. 5e, d and f, respectively. The Schmid factors for all the 12 FCC slip systems in grains of interest labeled A2-B2 and A3-B3 are reported in Table 1. Strain localization is observed in the form of a band of concentrated strain after the first cycle (Fig. 5a). The localized straining occurs on a plane parallel and near to the twin boundary of grains A2-B2. After 15% of the lifetime a second band of concentrated strain appears on the strain map parallel and close to the first band. After 45% of the lifetime, bands substantially increase in number and intensity. A crack is first detected at 45% of the lifetime in the same region where the band of concentrated strain was earlier observed during the cycling. The bands of concentrated strain observed near the twin boundaries are clearly associated with {111} slip planes of the highest Schmid factor slip system in grains A2-B2. The A2-B2 twin and parent grain pair has a parallel slip configuration [10], i.e. the {111} slip planes of the activated slip systems on one or both sides of the twin boundary are parallel to the twin boundary plane. Therefore, slip transmission across the twin boundary does not occur.

Fig. 6 reports the strain ε_{xx} along the profile indicated in Fig. 5c after fatigue testing for 1 cycle, 15% of lifetime, and 45% of lifetime. Arrows indicate the position of the most prominent strain bands in Fig. 5a and vertical dotted lines indicate the position of the twin boundary. After 1 cycle, compressive strain accumulates on one side of the twin boundary and is observed slightly offset from the twin boundary by 800 nm in the grain labeled A2 in Fig. 5e. After

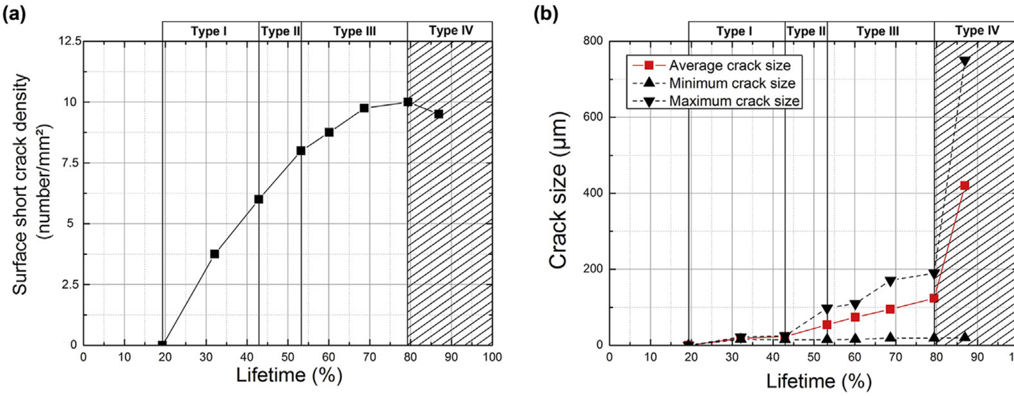

Fig. 3. Evolution during cycling of surface short crack density (a) and size (b) according the lifetime for fatigue cycling at maximum stress of 758 MPa.

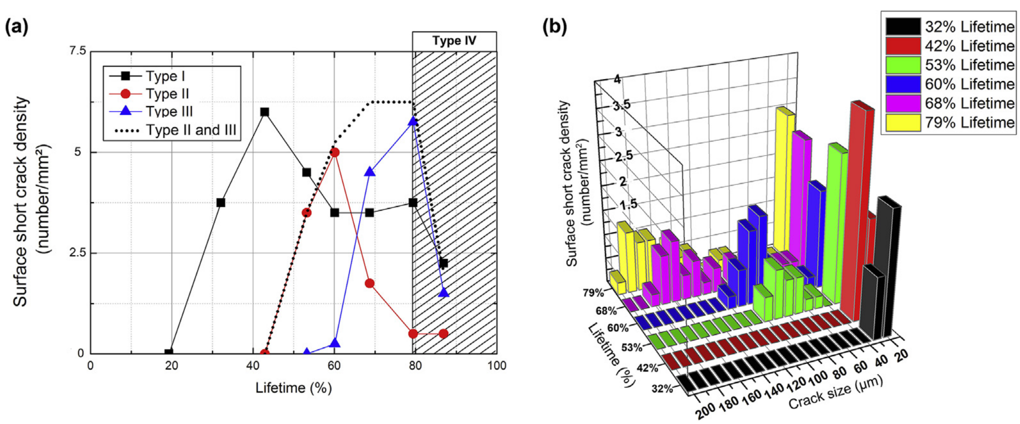

Fig. 4. (a) Evolution during cycling of Type I, II and III surface crack density. (b) Evolution of surface short crack density according the lifetime and crack size.

15% of the lifetime, a band of concentrated strain in tension is observed in addition to the compressive strain band and is offset from the twin boundary by 3 µm. After 45% of the lifetime, significant strain accumulation is observed near the twin boundary, corresponding to the crack observed on the associated SEM image in Fig. 5f.

3.1.2.2. Grain configurations favoring crack initiation. Fig. 7 presents two twin and parent grain pairs, A4-B4 and A5-B5, which initiated cracks during low cycle fatigue testing. SEM images in Fig. 7b and f show cracks after 45% of fatigue lifetime. The associated EBSD, highest Schmid factor, and elastic modulus maps which were obtained from the average crystallographic orientation of each grain along the loading direction and the compliance matrix of a nickel superalloy are presented for the grain A4-B4 in Fig. 7a, c and d respectively, and for grain A5-B5 in Fig. 7e, g and h, respectively. The slip systems with the highest Schmid factor in grains A4-B4 and A5-B5 are given in Fig. 7a and e, respectively. The Schmid factors for all the 12 FCC slip systems in grains of interest are reported in Table 1.

The twin and parent grain pairs A4-B4 and A5-B5 associated with initiation possess {111} slip planes of the activated slip systems on both sides of the twin boundary parallel to the twin boundary plane (parallel slip configuration [10]). Twin and parent grain A4-B4 have high maximum Schmid factors (0.498) whereas twin and parent grain A5-B5 have relatively lower maximum Schmid factors (0.437). In the twin and parent grain pair A4-B4 the elastic modulus in the twin and parent grain is similar and is accompanied by a high value of the maximum Schmid factor. However, in the relatively low maximum Schmid factor pair A5-B5 the twin and parent grain posses a low and high elastic modulus, respectively (and accordingly a high elastic modulus difference). In addition, the twin boundary for both pairs extends across the width of the grain and is longer than the average grain size of 26 µm.

Using fatigue tests interrupted at 80% of fatigue lifetime, 50 crack initiating twin and parent grain pairs were investigated using SEM and EBSD. For each twin and parent grain pair, maximum Schmid factor, elastic modulus of the twin and parent grain, and twin boundary length were calculated. Each twin and parent grain pair where cracks initiated exhibited a parallel slip configuration [10]. In this configuration the maximum Schmid factors of the twin and parent grain are identical. Therefore a single maximum Schmid factor can be considered for the twin and parent grain pair. Fig. 8a presents a histogram of twin boundary length for all twin and parent grain pairs, considering only pairs that result in crack initiation. Nearly all twins that are associated with crack initiation have a length well above the average grain size, often by a factor of 2–3 times. Additionally, no cracks initiate near twin boundaries shorter than 20 µm (just below the average grain size). Fig. 8b shows a histogram of maximum Schmid factor for all twin and parent grain pairs and only pairs where cracks initiated. X-axis values correspond to bin minima. Below a maximum Schmid factor of 0.43, no crack initiation was observed and high values of the maximum Schmid factor promote crack initiation.

Fig. 9a plots twin and parent grain orientations on a stereographic triangle according to the uniaxial loading direction, for pairs that initiate cracks by 80% of the lifetime (blue circles). Blue lines

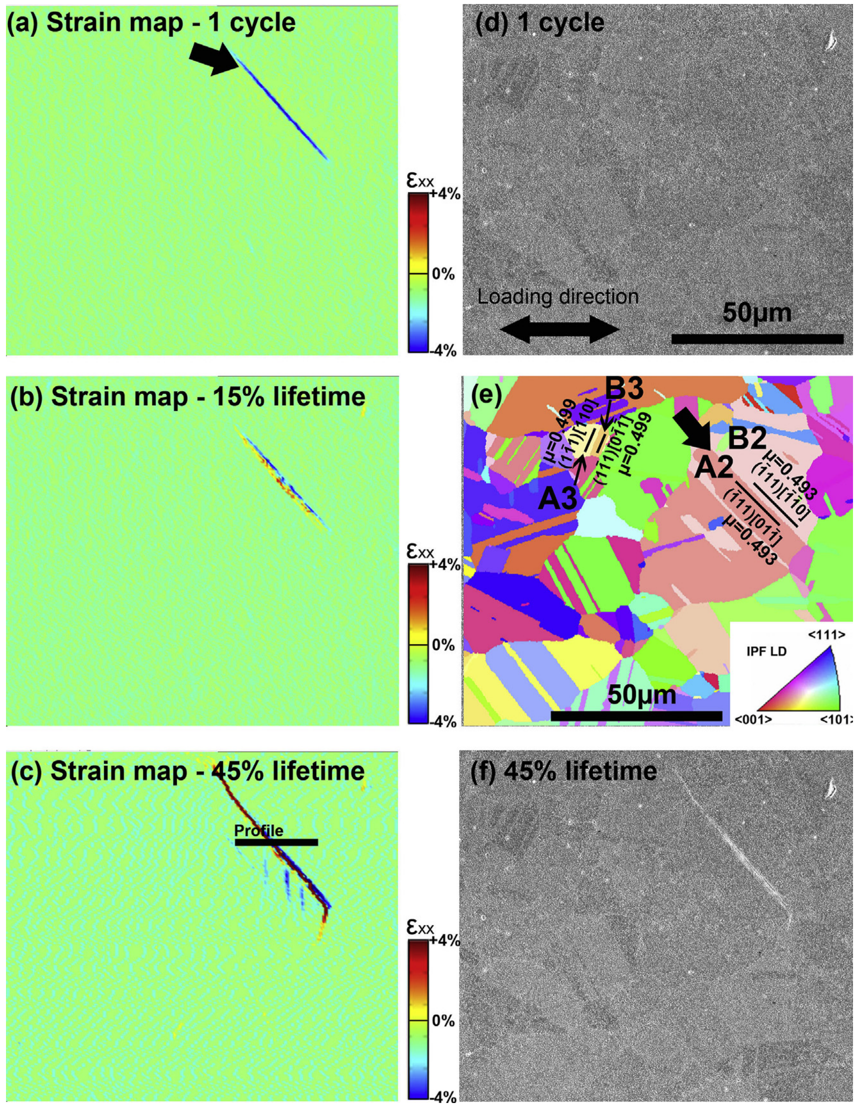

Fig. 5. Strain field ε_{xx} from DIC measurements after 1 cycle (a), 14% (b) and 45% (c) of the lifetime; associated SEM images after 1 cycle (d) and 45% of the lifetime (f); (e) associated EBSD map before loading.

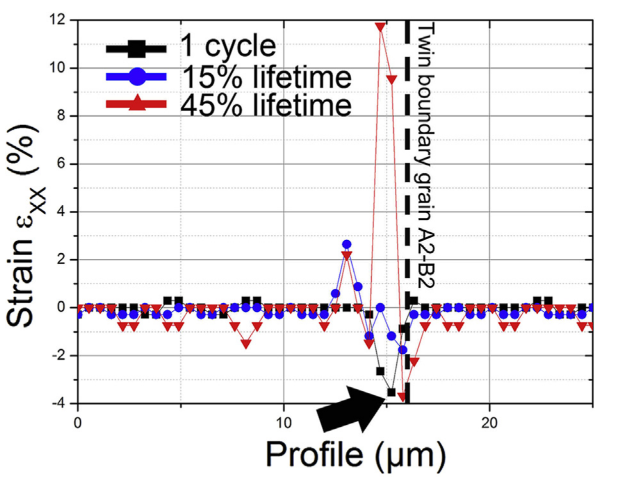

Fig. 6. Strain ε_{xx} along the profile depicted in Fig. 4c after 1 cycle, 15% and 45% of the lifetime during interrupted fatigue test. Vertical dotted lines indicate the position of the twin boundary along this profile. Arrows indicate the position of the main bands of concentrated strain in Fig. 4a.

connect twin and parent pairs. In addition, iso-curves of maximum Schmid factors and elastic modulus are indicated with black and red dashed curves, respectively. Fig. 9b shows maximum Schmid factor versus elastic modulus of the twin-parent grain pairs that result in crack initiation. Blue lines connect the twin and parent grain pairs. The black dashed line indicates the theoretical limit of the elastic modulus for a given maximum Schmid factor. In addition, 15 twin and parent grain pairs, which have a high Schmid factor, parallel slip configuration, and high twin boundary length, but did not initiate cracks have been investigated. For the sake of simplicity, only five of them are shown with red squares in Fig. 9a and b. Although high maximum Schmid factors promote crack initiation, twin and parent grain pairs with a relatively low maximum Schmid factor may still initiate a crack if they have a high disparity in elastic modulus.

Fig. 10a plots elastic modulus difference versus maximum Schmid factor for twin and parent grain pairs that initiate cracks after 80% of the lifetime. Depending on the maximum Schmid factor of the twin and parent grain pairs, there exists a threshold value of elastic modulus difference below which the twin and parent grain pairs do not initiate a crack (red area in Fig. 10a). None of the

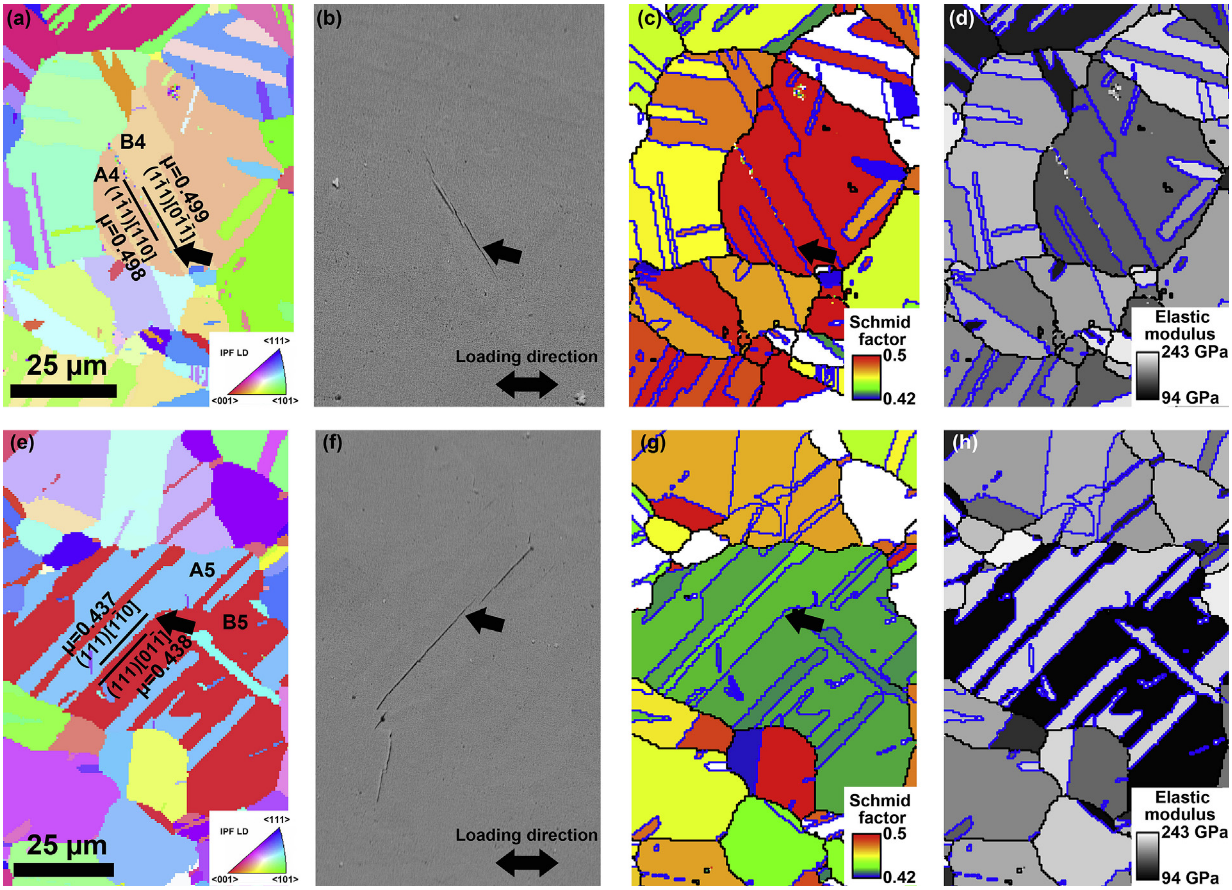

Fig. 7. Grains presenting crack after fatigue test interrupted at 45% of the lifetime: (a–e) inverse pole figure map; (b–f) associated SEM images; (c–g) associated highest Schmid factor map; (d–h) associated Elastic modulus map.

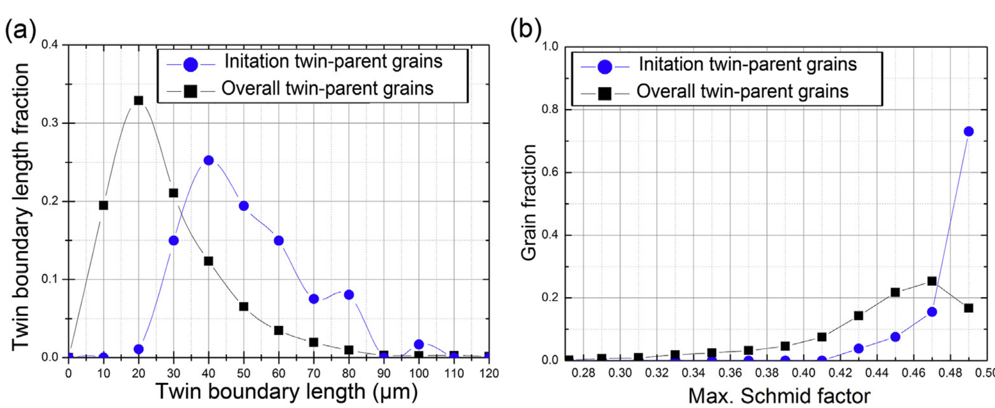

Fig. 8. (a) Twin boundary length fraction distribution according the twin boundary length for the overall twins and parent grain pairs and for the twins and parent grain pairs which present crack initiation at 80% of the lifetime; (b) twin and parent grain fraction distribution according the maximum Schmid factor.

investigated parallel slip configuration pairs (30 pairs) in the red area of Fig. 10a initiated a crack. It is noteworthy that the cracks always form on the elastically soft side of the pair.

Fig. 10b presents twin boundary length versus the maximum Schmid factor of the twin and parent grain pairs found to initiate a crack by 80% of the lifetime. Depending on the maximum Schmid factor of the twin and parent grain pair, there exists a threshold value of the twin boundary length, below which the twin and parent grain pairs do not initiate cracks (green area in Fig. 10b). All pairs investigated with a parallel slip configuration (30 pairs), falling in the green area in Fig. 10b, exhibit no crack initiation. In addition, 15 twin and parent grain pairs with a high Schmid factor, parallel slip configuration, and high elastic modulus difference but no crack initiation have been investigated. For the sake of simplicity, only five of them are reported with green squares in Fig. 10a and b. This demonstrates that both the elastic modulus variation and twin boundary length are critical parameters that promote crack initiation depending on the maximum Schmid factor.

Fig. 11 presents crack initiation pairs by their elastic modulus difference, maximum Schmid factor, and twin boundary length. All

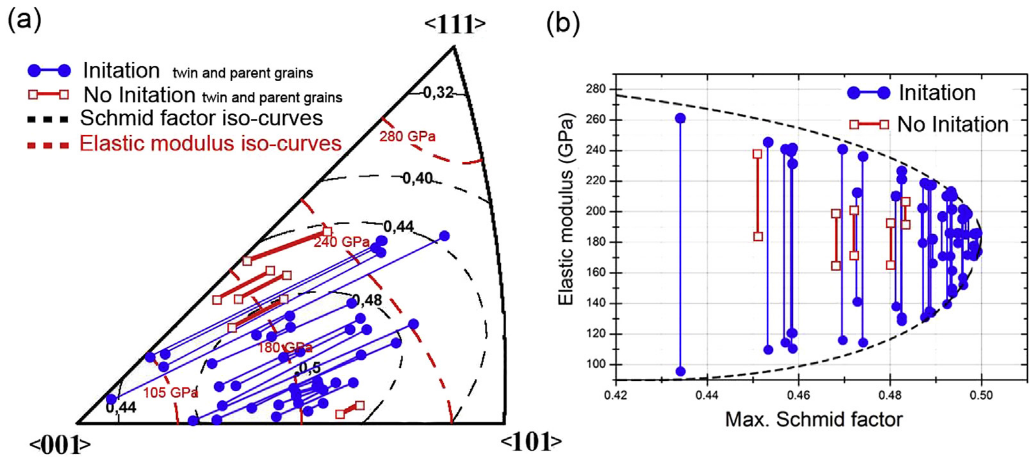

Fig. 9. (a) Inverse pole figure along the loading direction displaying the orientations of the twin and parent grain pairs which present crack initiation after 80% of the lifetime (blue circle); (b) Elastic modulus of the twins and parent grain according to their maximum Schmid factor for twin and parent grain pairs which present crack initiation after 80% of the lifetime (blue). (For interpretation of the references to colour in this figure legend, the reader is referred to the web version of this article.)

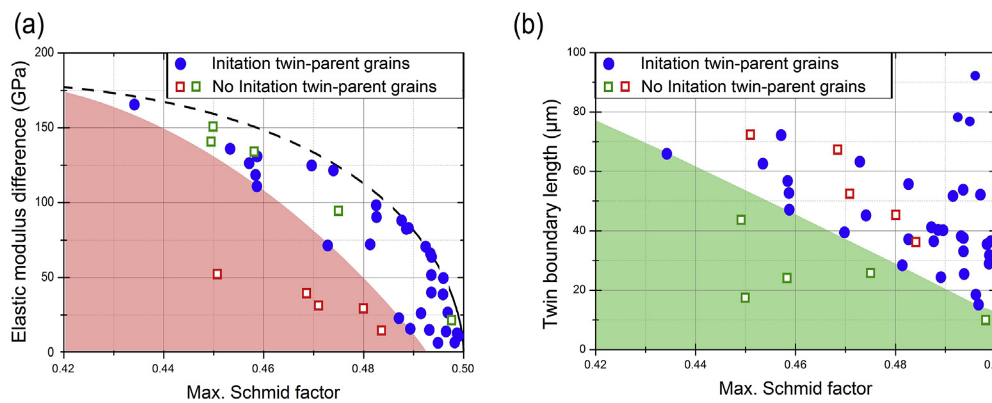

Fig. 10. (a) Elastic modulus difference according to the maximum Schmid factor of the twin and parent grain pairs which present crack initiation after 80% of the lifetime (blue circle), no crack initiation and high twin boundary length (red square), and no crack initiation and low twin boundary length (green square); (b) boundary length according to the maximum Schmid factor of the twin and parent grain pairs which present crack initiation after 80% of the lifetime (blue circle), no crack initiation and high twin boundary length (red square), and no crack initiation and low twin boundary length (green square). (For interpretation of the references to colour in this figure legend, the reader is referred to the web version of this article.)

investigated pairs (30) in the red domain in Fig. 11a and green domain Fig. 11b exhibit no crack initiation. All investigated pairs with cracks initiating by 80% of the lifetime fall within the blue domain in Fig. 11c.

3.2. Very high cycle fatigue regime

Very high cycle fatigue experiments were conducted with an ultrasonic fatigue apparatus that resonates samples at approximately 20 kHz [11]. Tests were conducted at room temperature with cyclic stress amplitudes in the range of 460–500 MPa. All fatigue specimens failed at lifetimes greater than 10^6 cycles within the very high cycle regime. Fatal cracks initiated at the surfaces of the specimens. As observed in the low cycle fatigue regime, all investigated cracks (50 secondary and fatal) initiated near a surface $\Sigma3$ twin boundary. In addition the slip systems with the highest resolved shear stress in both the twin and parent grain associated with the initiation site have their plane trace parallel to the twin boundary. Surface crack density has been measured after rupture on regions far from the fracture surface. An average crack density of 5.6 mm^{-2} was calculated for specimens tested in the very high cycle fatigue regime. Very high cycle fatigue specimens have a lower crack density than specimens tested in the low cycle fatigue regime (See Fig. 3). Additional details on the fatigue properties of the René 88DT in the very high cycle fatigue range can be found in Ref. [2].

Fig. 12a presents twin and parent pairs that initiated cracks in the very high cycle fatigue regime. For comparison, twin and parent pairs that initiated cracks in the low cycle fatigue regime are also reported. Fig. 12b plots twin and parent grain pairs found to initiate cracks on a stereographic triangle by their loading axis. Twin and parent grain pairs are connected by a green line. In addition, iso-curves of the maximum Schmid factor and elastic modulus are denoted with black and red dashed curves, respectively. Fig. 12c and d plot the elastic modulus difference and twin boundary length versus the maximum Schmid factor of the twin and parent grain pairs. Regions for which no crack initiation pairs were observed in the low cycle fatigue regime (Fig. 10) are indicated in green and red for comparison.

As observed in the low cycle fatigue regime, there is a threshold elastic modulus difference and twin boundary length for each Schmid factor below which the twin and parent grain pairs do not

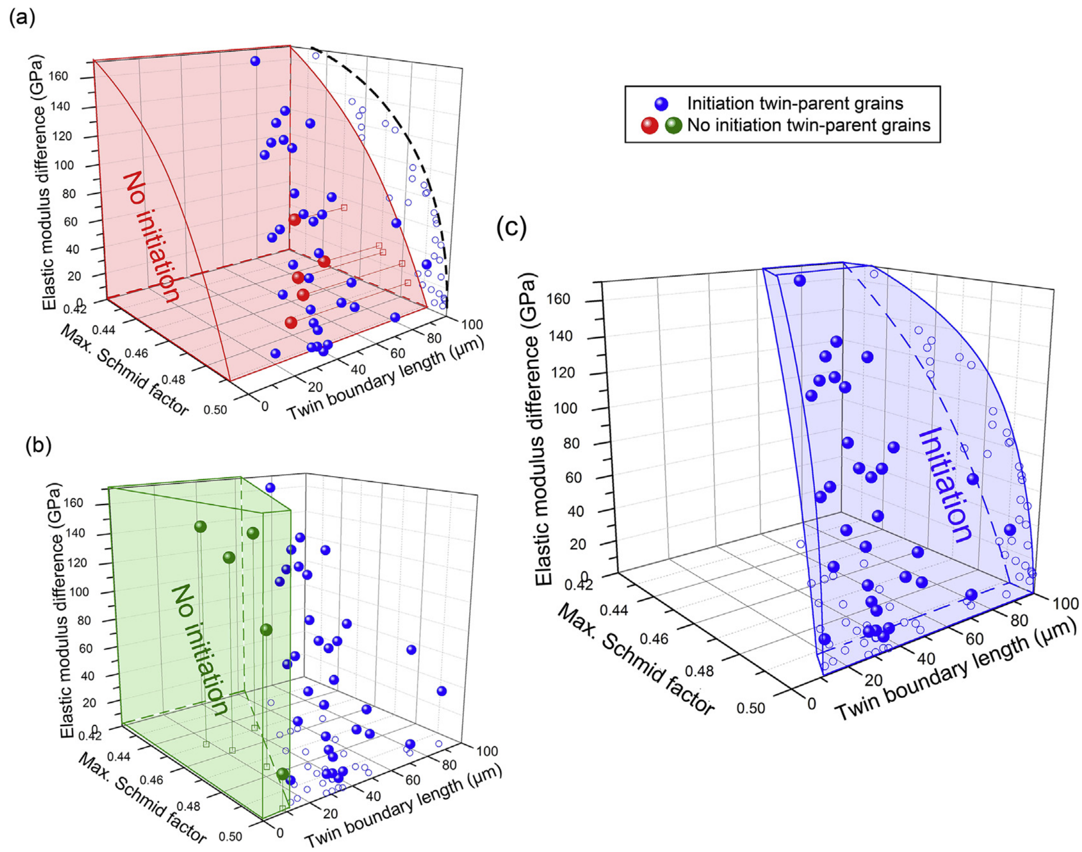

Fig. 11. Twin and parent grain pairs which present crack initiation (blue sphere), no crack initiation and high twin boundary length (red sphere), and no crack initiation and low twin boundary length (green sphere); (a) critical domain (red area) where no crack initiation has been reported due to the low elastic difference; (b) critical domain (green area) where no crack initiation has been reported due to the low twin boundary length; (c) domain (blue area) where parallel slip configuration twin and parent grain pairs present crack initiation. Open circles present the projection of the pairs on the X,Y-axis plane and X,Z-axis plane. (For interpretation of the references to colour in this figure legend, the reader is referred to the web version of this article.)

initiate cracks. High maximum Schmid factors, longer twins and high elastic modulus difference grain pairs promote crack initiation in the very high cycle fatigue regime. It is important to note that the elastic modulus difference threshold for a given Schmid factor is higher in the very high cycle fatigue regime compared to the low cycle fatigue regime, indicating that elastic modulus difference is a more critical parameter in the very low cycle fatigue regime.

Considering the slip system with the highest Schmid factor in a parallel slip configuration (Fig. 13b), i.e. the slip system with its plane parallel to the coherent twin boundary, the angle between the Burgers vector (slip direction – see b_{twin} and b_{pg} in Fig. 13b) and the surface trace of the twin boundary (see $t_{twin\ boundary}$ in Fig. 13b) is identical for the slip system in the twin and the parent grains. Thus, in a parallel slip configuration, a unique angle can be used to describe the twin and parent grain. Fig. 13a presents this angle for twin and parent grain pairs found to initiate cracks in the very high cycle fatigue. The same data is shown for low cycle fatigue for comparison. The slip direction with the highest resolved shear stress within most twin and parent grain pairs forms a relatively small angle (less than 40°) with respect to the boundary trace in the very high cycle regime. The same holds in the low cycle fatigue regime for twin and parent grain pairs with a relatively low maximum Schmid factor.

In addition to the low cycle and very high cycle fatigue tests, two cyclic deformation tests were performed on cylindrical specimens in air under load control conditions at maximum stress of 758 MPa with a R-ratio of 0.1 and a frequency of 1 Hz at room temperature. At R-ratio of 0.1 i.e. without compressive phase during the cycling, the two specimens did not fail and reached 10^6 cycles where the test was interrupted.

4. Discussion

Quantitative analysis of crack size and density during fatigue cycling has been conducted for a polycrystalline nickel-based superalloy René 88DT (Figs. 3 and 4). Multiple cracks nucleate and propagate simultaneously during cycling. Of particular interest for this alloy, which contains a high density of annealing twins, is that all cracks initiate near coherent twin boundaries at the stress levels investigated in the LCF and VHCF regime. Therefore this alloy is an obvious candidate for understanding the role of the microstructure in crack initiation mechanisms at twin boundaries. Crystallographic orientation, grain shape and size, and neighboring microstructure are relevant parameters for the crack initiation process [1,7,11,12,14,15]. At the microscopic scale crack initiation is dominated by localization of plastic strain in persistent slip bands (PSBs) [25–28]. Moreover, interaction of dislocations with interfaces (grain and twin boundaries) is also critical for the advancement of grain-scale cracks into grains surrounding the initiation grain [7]. In the case of a fcc material containing coherent twins, the twin boundary is parallel to a slip plane. Therefore a parallel slip configuration (Fig. 13b) where an activated slip plane is parallel to the twin plane may be present. Without transmission across twin boundaries, dislocations glide on a highly stressed, twin-parallel slip system, remaining in the original grain near the twin boundary. Heinz and Neumann [7], observing crack initiation in stainless

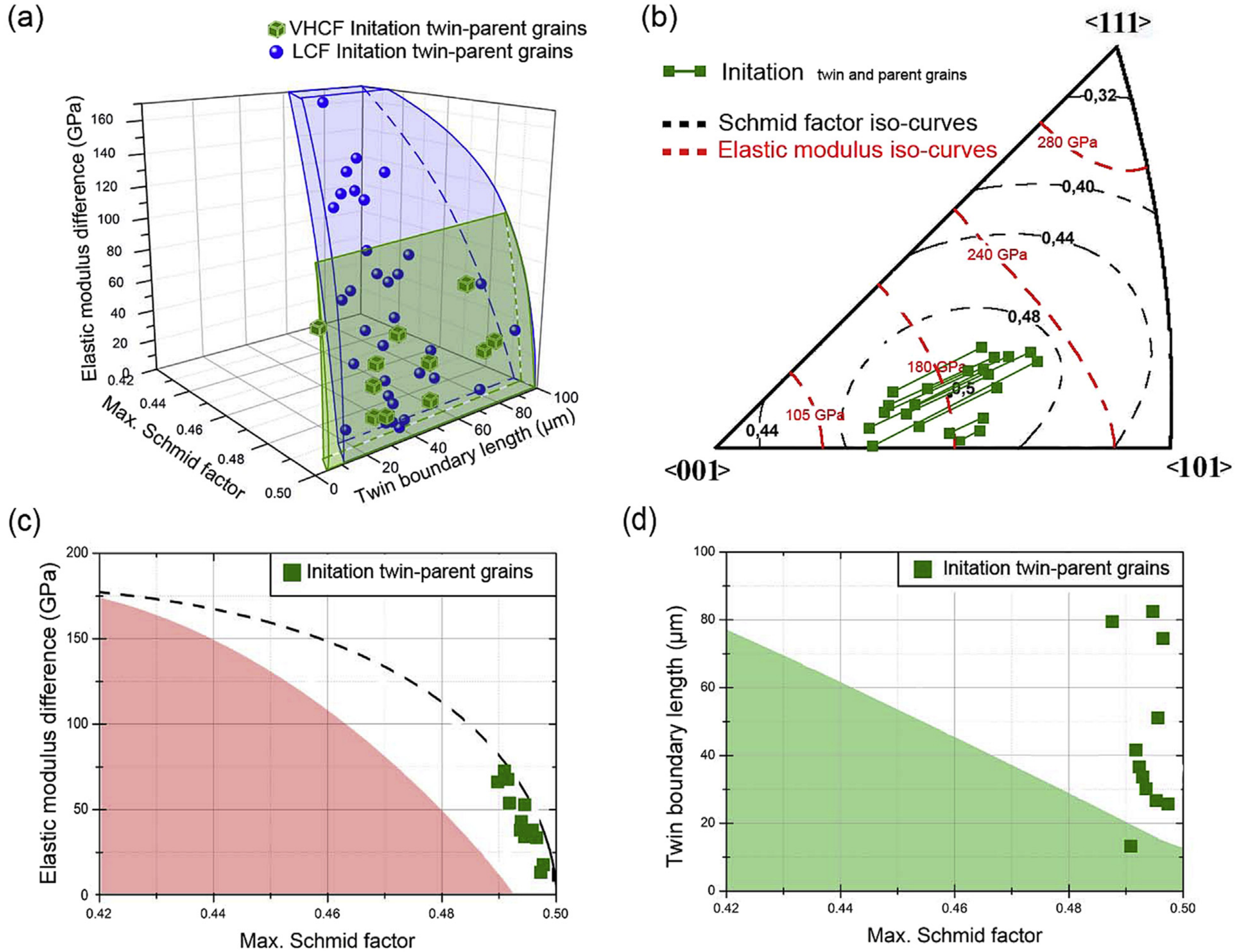

Fig. 12. (a) Twin and parent grain pairs which present crack initiation in the very high cycle regime (green cube) and in the low cycle fatigue regime (blue sphere); critical domain where parallel slip configuration twin and parent grain pairs present crack initiation in the very high cycle regime (green area) and in the low cycle regime (blue area); (b) Inverse pole figure along the loading direction displaying the orientations of the twin and parent grain pairs, which present crack initiation in the very high cycle fatigue regime; (c) Elastic modulus difference and (d) boundary length of the twin and parent grain, which present crack initiation, according to the maximum Schmid factor. (For interpretation of the references to colour in this figure legend, the reader is referred to the web version of this article.)

steel at twin boundaries, first suggested that elastic anisotropy causes local stress concentrations, strongly supporting glide adjacent to twin boundaries. This leads to stronger strain localization than a general grain boundary with oblique slip planes [7]. An activated slip system parallel to a twin boundary (possible with a coherent twin boundary and parallel slip configuration) allows for dislocations to travel relatively long distances unhindered, creating high local strains and correspondingly high incompatibility stresses at

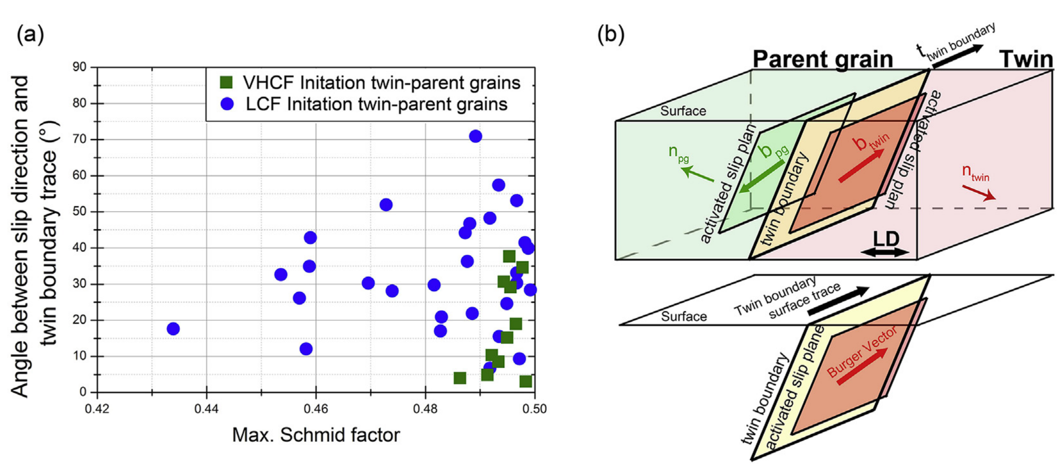

Fig. 13. (a) Angle between slip direction of the slip system with the maximum Schmid factor and the twin boundary surface trace for twin and parent grain pair, which present crack initiation during very high cycle fatigue test (green square) and during low cycle fatigue (blue circle), according the maximum Schmid factor. (b) Parallel slip configuration twin and parent grain pair. (For interpretation of the references to colour in this figure legend, the reader is referred to the web version of this article.)

the boundary. Tschopp et al. [29], using atomistic calculations, predicted that the lowest stresses required for dislocation nucleation occur at coherent twin boundaries. Stein, Rollett, Ingraffea et al. [8,9], using a crystal plasticity model report very high stresses near twin boundaries in Ni-base alloys in the parallel slip configuration. Miao et al. [2] and Stinville et al. [10] experimentally detect high shear strains in the vicinity of twin boundaries in René 88DT during straining with an enhanced local plastic straining in the parallel slip configuration below yielding in compression [10]. The present work also shows compressive strain accumulation (Fig. 5a) after the first cycle near twin boundaries in the parallel slip configuration. Despite a relatively low stress level (below yielding), slip occurs during the compressive phase of the first cycle due to an enhanced local plastic straining near twin boundaries in compression [10]. Strain accumulation in tension is observed near twin boundaries (Fig. 5b) in addition to this compressive strain accumulation during cycling. This strain accumulation in tension may be the signature of persistent slip bands (PSB), which lead to crack initiation after subsequent cycling (Fig. 5f). Strain localization in the earliest stages of cycling and the irreversible accumulation of strains is strongly enhanced by the presence of the γ' precipitates [37]. The PSBs observed are thinner than in single-phase materials, and strain localization is significantly higher in magnitude [38,39]. As a consequence, the extrusion effect can be very large [37] as observed in Fig. 2.

Fatigue specimens tested at R-ratio of 0.1 with a maximum stress level of 758 MPa present significantly higher lifetimes (higher than 10^6 cycles) compared to specimens tested at R-ratio of −1, indicating that the compressive phase of the cycle induces strain localization after the first cycle near specific twin boundaries, resulting PSBs during subsequent cycling, and ultimately crack initiation. As the precipitate structure of the René 88DT affects the strain localization, the lattice misfit existing between the two phases may promote the shearing of precipitates in compression.

4.1. Critical condition for crack initiation

Cracks preferentially initiate in a grain with a high maximum Schmid factor (calculated assuming uniaxial loading) as shown in Fig. 8b. Favorably oriented grains have a high resolved shear stress on the slip system parallel to the twin boundary, inducing early plasticity, which accumulates during cycling. However, not all twin boundaries with a parallel slip configuration and high maximum Schmid factor initiate cracks, indicating that other parameters are important. For example, both grain pairs A2-B2 and A3-B3 in Fig. 5e have a highly stressed plane parallel to the twin boundaries, but only the pair A2-B2 pair initiates a crack.

Fig. 10b indicates that a critical twin boundary length is necessary for crack initiation. Previous studies in nickel [30], copper [5,6], and steel [4] clearly indicate that grain size influences cyclic plasticity and fatigue crack initiation mechanisms. The fatigue crack initiation model proposed by Tanaka and Mura [31] and later refined by Lin et al. [32] and Mura and Nakasone [33], describes fatigue crack initiation by the accumulation of dislocation dipoles during cycling. This model predicts that the number of cycles for crack initiation is proportional to $(1/\mathbf{a})$ where $\mathbf{a}$ is the length of the slip plane in a grain. The irreversibility of dislocation motion yields a systematic increase in the dislocation density in pileups during cycling. The total number of dislocations accumulated is proportional to $\mathbf{a}$ i.e. the length of the slip plane dislocation [32]. It is therefore reasonable to conclude that the length of the twin boundary affects crack initiation, since they are correlated in the parallel slip configuration. In addition, it appears that the critical twin boundary length for crack initiation depends on the maximum Schmid factor as shown in Fig. 10b. Even relatively lower Schmid factor twin and parent grain pairs can initiate a crack if the twin boundary has sufficient length.

Another major parameter influencing crack initiation is the elastic modulus difference between the twin and parent grain. Figs. 10a and 12c indicates that, for relatively low Schmid factors, a high difference in elastic modulus is necessary to initiate a crack near the boundary in the elastically soft twin or parent grain. Elastic anisotropy at the twin boundary causes a local stress concentration during straining [7], favoring plasticity near twin boundaries. Strain field heterogeneities at the grain-scale induced by the elastic anisotropy associated with the coherent twin will be addressed experimentally in a future paper using sub-grain DIC measurements (see Ref. [17]). Heinz and Neumann [7] have extensively explored the role of elastic anisotropy and argue that elastic anisotropy and coherency of the twin are decisive. They proposed a model to evaluate local stress concentrations in the vicinity of twin boundaries based on the elastic anisotropy [34]. From the calculated results, they concluded that twin boundaries do not crack, but act as stress raisers, promoting the formation of PSBs. In the present paper, using DIC measurements, it is reported that cracks initiate, not at the exact location of the twin boundary, but slightly offset (Fig. 6). Strain localization appears adjacent to the twin boundary indicating the presence of PSBs (Fig. 5b). More recently Stein, Rollett, and Ingraffea et al. [8,9] have shown by crystal plasticity calculations that the resolved shear stresses at twin boundaries with a parallel slip configuration (Fig. 13b) result in a low and high stress state on either side of the twin boundary, respectively. They suggest this could be due to enhanced localized shearing. For fcc twin boundaries, with a misorientation of 60° between the twin and the parent grain, the elastic modulus difference in the twin and parent grain pairs can be significant, inducing a local stress concentration close to the twin boundary. For a high elastic modulus difference, the high elastic anisotropy associated with a superalloy (Zener elastic anisotropy ratio higher than 2) enhances local stresses and may induce nucleation of a PSB. For grains with a very high Schmid factor, the elastic modulus difference between the twin and parent grain in parallel slip configuration is low. However, for twin and parent grains with relatively lower Schmid factors, the difference can be significant. In this later case, even relatively low Schmid factor pairs can initiate a crack (Fig. 10a).

Depending on the maximum Schmid factor, both elastic modulus difference and twin boundary length significantly affect the initiation process in both the very high and low cycle fatigue regimes. A critical domain (high maximum Schmid factor, high elastic modulus difference and high twin boundary length) can be defined to predict twin and parent grain pairs amenable to crack initiation. Fig. 12a presents twin and parent pairs which initiate cracks in the very high and low cycle fatigue regimes. The crack initiation domain for very high cycle fatigue is contracted in comparison to the domain for low cycle fatigue regime. This is in agreement with the lower experimentally observed crack density in the very high cycle fatigue regime (2 times lower compared to the crack density in the low cycle fatigue regime). The length of the twin boundary has the same effect on crack initiation in both regimes. An elastic modulus difference in the very high cycle fatigue regime is necessary to initiate a crack, indicating that elastic modulus difference and, by extension, elastic anisotropy are also critical parameters for lower stresses. For the very high cycle fatigue regime (Fig. 12c) most cracks initiate in grain pairs with a maximum Schmid factor around 0.495 and high elastic modulus difference. This indicates that pairs with higher Schmid factor but lower elastic modulus difference may not initiate a crack, suggesting that a high elastic modulus difference is critical for initiation in the very high cycle fatigue regime, which in this study spans up to 45% of the yield strength.

Interestingly, the slip direction with the highest resolved shear stress within most twin and parent grain pairs forms a small angle (less than 40°) with respect to the boundary trace for initiated pairs in the very high cycle regime (Fig. 13). The same point can be made in the low cycle fatigue regime for relatively low maximum Schmid factor twin and parent grain pairs (Fig. 13). The Burgers vector of the dislocations in this configuration is nearly parallel to the free surface, and thus aligned with the trace of twin boundary on the specimen surface. In this configuration, the dislocation slip along the slip plane will not generate significant steps (extrusion–intrusion) at the free surface. Under cyclic loading the shear deformation resulting from previous step cannot be completely recovered due to the irreversible nature of the dislocation slip processes [35], leading to accumulation of cyclic strain localization at the intersection of the slip band with the edge of the grain. Because this kind of cyclic strain localization does not involve the formation of high amplitude extrusions, the irreversibility of dislocation motion results in a systematic pileup of dislocations at the intersection of the slip band with the neighboring grain on the slip system parallel to a favorable twin boundary. This could enhance slip in the neighboring grain and favor initiation and propagation of damage [10].

4.2. Crack distribution function

A new approach for analyzing crack initiation parameters has been performed using a crack distribution function (CDF). This function evaluates the fraction of initiated twin and parent grain pairs for the microstructural parameters affecting crack initiation: (1) maximum Schmid factor (μ_{max}), (2) elastic modulus difference (ΔE), (3) length of twin boundary (L), angle between slip direction and twin boundary surface trace (θ). The CDF (μ_{max}, ΔE, L, θ) for a set of (μ_{max}, ΔE, L, θ) is equal to the fraction of crack initiating twin and parent grain pairs with a maximum Schmid factor in the domain [$\mu_{max} - d\mu_{max}$, $\mu_{max} + d\mu_{max}$], a elastic modulus difference in [$\Delta E - d\Delta E$, $\Delta E + d\Delta E$], a twin boundary length in [L – dL, L + dL], and a angle between the slip direction and the surface twin boundary trace in [$\theta - d\theta$; $\theta + d\theta$].

Fig. 14a and b plots this function against elastic modulus difference and the maximum Schmid factor for low cycle and very high cycle fatigue, respectively for a sampling of $d\mu_{max}$ equal to 0.03 and $d\Delta E$ equal to 15 GPa. Statistical analysis has been performed on all investigated cracks in the very high cycle (50 cracks) and low cycle (50 cracks) fatigue regime. Two distinct peaks appear in the low cycle fatigue regime. The first one is characterized by a very high maximum Schmid factor. The second falls on a relatively high Schmid factor (around 0.49) and a relatively high elastic modulus difference (around 75 GPa). In the very high cycle fatigue regime, a single peak with a relatively high maximum Schmid factor (around 0.495) and an elastic modulus difference of approximately 30 GPa. The very high cycle fatigue regime occurs at a lower maximum Schmid factor than the first low cycle fatigue regime peak, confirming that an additional driving force is required; a high elastic modulus difference is thus critical for initiation in the very high cycle fatigue regime. Two families of cracks can be observed in the low cycle fatigue regime, the first has a very high maximum Schmid factor resulting in a large resolved shear on the slip system parallel to the twin boundary. The second family is characterized by twin and parent grain pairs with relatively high Schmid factors and a high elastic modulus difference. The high elastic modulus difference increases shear stress near the twin boundary due to the elastic anisotropy, increasing the resolved shear stress on the twin parallel slip system accordingly. High elastic modulus difference induced a significant strain enhancement near the twin boundaries [17] during the elastic loading part of the cycle. Subsequently, early plasticity occurred at these locations as the sample approached the yield strength. In the very high cycle regime (Fig. 14b), twin and parent grain pairs with a very high Schmid factor (close to 0.5) do not necessary initiate cracks due to the low elastic modulus difference. Therefore elastic anisotropy is the crucial factor for stresses significantly below the elastic limit. A high elastic modulus difference enhances strain near the twin boundaries [17], which induces the development of localized plasticity during cycling on the highly stressed slip system.

These criteria can be applied to either 2-D or 3-D sections of material. For example, in a 2-D EBSD scan measuring 1000 by 1500 μm (total of 4960 pairs) less than 0.02% of pairs would satisfy the criteria for initiation in the very high cycle regime.

Finally, we note that the criteria developed here are extracted from two-dimensional sections through the microstructure. Neighboring grains will clearly influence the resolved shear stresses in slip systems. Considering grains to be uniaxially loaded for the calculation of the resolved shear stress (Schmid factor) is a significant assumption, since the local stress at the boundary can be affected by the surrounding microstructure configuration. This assumption will be examined in more detail in a future publication using full 3-D datasets and elastic–plastic modeling approaches [40]. However, this simple hypothesis gives a good prediction of the location of initial crack initiation sites, with application of a combined criterion that considers Schmid factor, Burgers vector configuration, elastic anisotropy and twin boundary length.

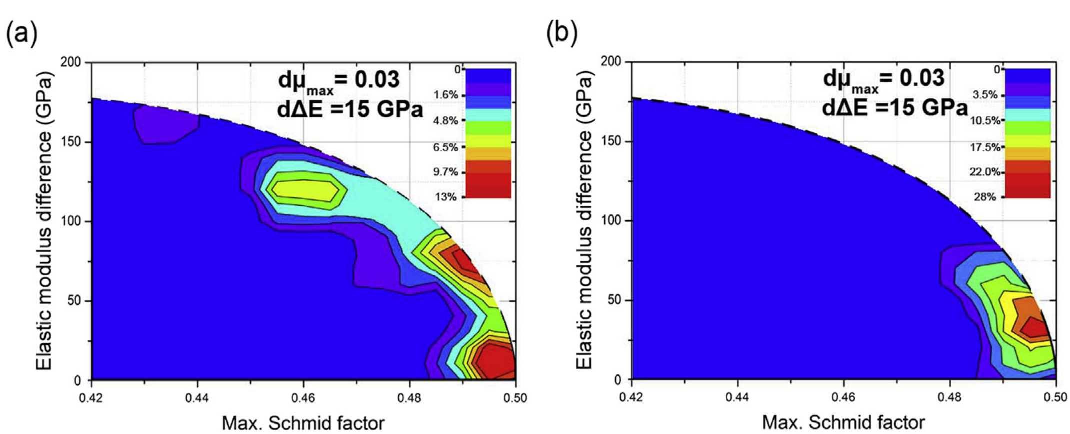

Fig. 14. Initiated twin and parent grain pair fraction according their elastic modulus difference and their maximum Schmid factor for the low (a) and very high (b) cycle fatigue regime.

5. Conclusion

The fatigue behavior of a polycrystalline nickel-base superalloy René 88DT was investigated under fully reversed loading in the very high and low cycle fatigue regimes. Regions close to favorably oriented, surface twin and parent grain pairs are dominant sites for fatigue crack initiation.

The critical domain for crack initiation in twin-containing fcc materials has been bounded as a function of the elastic modulus difference, the Schmid factor, and the twin boundary length in order to predict crack initiation.

Using high resolution digital image correlation and the crack distribution function, elastic anisotropy has been demonstrated to have a significant effect on the crack initiation process in the low cycle and very high cycle fatigue regimes. In addition, the orientation of the slip direction with the highest resolved shear stress within most twin and parent grain pairs with respect to the boundary trace has a significant influence on the initiation process in the very high cycle regime.

Acknowledgments

The authors gratefully acknowledge the support of GE Global Research, AFOSR/AFRL for sponsoring Center of Excellence on Integrated Materials Modeling (CEIMM – Grant FA9550-12-1-0445) and the Air Force Center of Excellence (Grant FA9550-12-1-0445) and appreciate useful discussions with J. Laflen and A. Loghin.

References

[1] J. Miao, T.M. Pollock, J.W. Jones, Crystallographic fatigue crack initiation in nickel-based superalloy René 88DT at elevated temperature, Acta. Mater. 57 (2009) 5964–5974.
[2] J. Miao, T.M. Pollock, J.W. Jones, Microstructural extremes and the transition from fatigue crack initiation to small crack growth in a polycrystalline nickel-base superalloy, Acta. Mater. 60 (2012) 2840–2854.
[3] C. Stein, S. Lee, A. Rollett, An Analysis of Fatigue Crack Initiation Using 2D Orientation Mapping and Full-field Simulation of Elastic Stress Response, Superalloys 2012, 2012, Champion, PA.
[4] M. Mineur, P. Villechaise, J. Mendez, Influence of the crystalline texture on the fatigue behavior of a 316L austenitic stainless steel, Mat. Sci. Eng. A 286 (2000) 257–268.
[5] N. Thompson, N. Wadsworth, N. Louat, The origin of fatigue fracture in copper, Philos. Mag. 1 (1956) 113–126.
[6] R.C. Boettner, A.J. McEvily, Y.C. Liu, On the formation of fatigue cracks at twin boundaries, Philos. Mag. 10 (1964) 95–106.
[7] A. Heinz, P. Neumann, Crack initiation during high cycle fatigue of an austenitic steel, Acta. Metall. Mater. 38 (1990) 1933–1940.
[8] C.A. Stein, A. Cerrone, T. Ozturk, S. Lee, P. Kenesei, H. Tucker, R. Pokharel, J. Lind, C. Hefferan, R.M. Suter, A.R. Ingraffea, A.D. Rollett, Fatigue crack initiation, slip localization and twin boundaries in a nickel-based superalloy, Curr. Opin. Solid State Mater. Sci. 18 (2014) 244–252.
[9] A. Cerrone, A. Spear, J. Tucker, C. Stein, A. Rollett, A. Ingraffea, Modeling crack nucleation at coherent twin boundaries in nickel-based superalloys, Mat. Sci. Tech. (2013) 1649–1656, 2013 MS&T.
[10] J.C. Stinville, N. Vanderesse, F. Bridier, P. Bocher, T.M. Pollock, High resolution mapping of strain localization near twin boundaries in a nickel-base superalloy, Acta. Mater. Acta. Mater. 98 (2015) 29–42.
[11] A. Shyam, C.J. Torbet, S.K. Jha, J.M. Larsen, M.J. Caton, C.J. Szczepanski, et al., Development of ultrasonic fatigue for rapid, high temperature fatigue studies in turbine materials, in: K.A. Greeen, H. Harada, T.E. Howson, T.M. Pollock, R.C. Reed, J.J. Schirra, et al. (Eds), Superalloys 2004, The Minerals, Metals & Materials Society, Warrendale (PA), 2004, pp. 259–268.
[12] J.C. Healy, L. Grabowski, C.J. Beevers, Short-fatigue-crack growth in a nickel-base superalloy at room and elevated temperature, Fatigue Fract. Eng. Mater. Struct. 15 (1992) 309.
[13] R.G. Tryon, A. Dey, G. Krishnan, K.S.R. Chandran, M. Oja, Identifying sensitive parameters at fatigue crack nucleation sites using microstructural simulation models, in: J.M. Larsen, L. Christodoulou, J.R. Calcaterra, M.L. Dent, M.M. Derriso, W.J. Hardman, et al. (Eds.), Materials Damage Prognosis – Proceedings of a Symposium of the Materials Science and Technology 2004 Conference, The Minerals, Metals, & Materials Society, 2004, p. 105.
[14] K. Li, N.E. Ashbaugh, A.H. Rosenberger, Crystallographic initiation of nickel-base superalloy IN100 at RT and 538°C under low cycle fatigue conditions, in: K.A. Greeen, H. Harada, T.E. Howson, T.M. Pollock, R.C. Reed, J.J. Schirra, et al. (Eds), Superalloy 2004, The Minerals, Metals & Materials Society, Warrendale (PA), 2004, p. 251.
[15] D.L. Davidson, R.G. Tryon, M. Oja, R. Matthews, K. Chandran, S. Ravi, Fatigue crack initiation in WASPALOY at 20 °C, Metall. Mater. Trans. A 38 (2007) 2214.
[16] S.L. Wong, P.R. Dawson, Influence of directional strength-to-stiffness on the elastic–plastic transition of fcc polycrystals under uniaxial tensile loading, Acta. Mater. 58 (2010) 1658–1678.
[17] J.C. Stinville, M.P. Echlin, D. Texier, F. Bridier, P. Bocher, T.M. Pollock, Sub-grain scale digital image correlation by electron microscopy for polycrystalline materials during elastic and plastic deformation, Exp. Mech. (2015) http://dx.doi.org/10.1007/s11340-015-0083-4.
[18] D.D. Krueger, R.D. Kissinger, R.G. Menzies, Development and introduction of a damage tolerant high temperature nickel-base disk alloy, Rene 88DT, in: S.D. Antolovich (Ed.), Superalloys 1992, TMS-AIME, Warrendale, PA, 1992, pp. 277–286.
[19] S.T. Wlodek, M. Kelly, D.A. Alden, The structure of Rene 88 DT, in: R.D. Kissinger, D.J. Deye, D.L. Anton, A.D. Cetel, M.V. Nathal, T.M. Pollock, D.A. Woodford (Eds.), Superalloys 1996, The Miner. Metals Mater. Society, 1996.
[20] J. Miao, T.M. Pollock, J.W. Jones, Fatigue crack initiation in nickel-based superalloy René 88 DT at 593°C, in: R.C. Reed, K.A. Green, P. Caron, T.P. Gabb, M.G. Fahrmann, E.S. Huron, S.A. Woodard (Eds.), Superalloys 2008, TMS, 2008.
[21] A. Tatschl, O. Kolednik, A new tool for the experimental characterization of micro-plasticity, Mater. Sci. Eng. A 339 (2003) 265–280.
[22] F. Bridier, J.C. Stinville, N. Vandresse, P. Villechaise, P. Bocher, Microscopic strain and crystal rotation measurement within metallurgical grains, Key Eng. Mater. 592–593 (2014) 493–496.
[23] B. Pan, K. Qian, H. Xie, A. Asundi, Two-dimensional digital image correlation for in-plane displacement and strain measurement: a review, Meas. Sci. Technol. 20 (2009) 1.
[24] A. Bataille, T. Magnin, Surface damage accumulation in low-cycle fatigue, Acta. Metall. Mater. 42 (1994) 3817–3825.
[25] H. Mughrabi, R. Wang, Cyclic stress–strain response and high cycle fatigue behaviour of copper polycrystals, in: 46, Basic Mechanisms in Fatigue of Metals, Mater. Sci. Monographs, 1988, pp. 1–14.
[26] C. Laird, D.J. Duquette, Mechanisms of fatigue crack nucleation, in: Corrosion Fatigue, National Association of Corrosion Engineers, 1972, pp. 88–117.
[27] C.A. Stubbington, P.J.E. Forsyth, Some observations on microstructural damage produced by fatigue of an aluminium-7.5% zinc-2.5% magnesium alloy at temperatures between room temperature and 250°C, J. Instit. Met. 86 (1957/58) 90–94.
[28] M. Bayerlein, H. Mughrabi, Fatigue crack initiation and early crack growth in copper polycrystals – effects of temperature and environment, in: Short Fatigue Cracks, ESIS 13, Mech. Eng. Publications, 1992, pp. 55–82.
[29] M.A. Tschopp, G.J. Tucker, D.L. McDowell, Atomistic simulations of tension–compression asymmetry in dislocation nucleation for copper grain boundaries, Comput. Mater. Sci. 44 (2008) 351–362.
[30] D.J. Morrison, J.C. Moosbrugger, Effects of grain size on cyclic plasticity and fatigue crack initiation in nickel, Int. J. Fatigue 19 (1997) 851–859.
[31] K. Tanaka, T. Mura, A dislocation model for fatigue crack initiation, J. Appl. Mech. 48 (1981) 97–103.
[32] M.R. Lin, M.E. Fine, T. Mura, Fatigue crack initiation on slip bands: theory and experiment, Acta Metal. 34 (1986) 619–628.
[33] T. Mura, Y. Nakasone, A theory of fatigue crack initiation in solids, J. Appl. Mech. 57 (1990) 1–6.
[34] P. Neumann, Analytical solution for the incompatibility stresses at twin boundaries in cubic crystals, Fatigue 99 (1999) 107–114.
[35] H. Mughrabi, Cyclic slip irreversibilities and the evolution of fatigue damage, Met. Mater. Trans. B 40 (2009) 1257–1279.
[36] H. Mayer, Fatigue crack growth and threshold measurements at very high frequencies, Int. Mater. Rev. 44 (1999) 1–34.
[37] H. Mughrabi, Specific features and mechanisms of fatigue in the ultrahigh-cycle regime, Inter. J. Fatigue 28 (2006) 501–508.
[38] C. Laird, The Application of Dislocation Concepts in Fatigue, in: F.R.N. Nabarro (Ed), Dislocations in Solids, 6, North-Holland Publishing Company, New York, NY, 1983, pp. 57–120.
[39] J.K. Lee, C. Laird, Strain localization during fatigue of precipitation hardened aluminium alloys, Phil. Mag. A 47 (1997) 579–597.
[40] M.P. Echlin, M. Straw, S. Randolph, J. Filevich, T.M. Pollock, The tribeam system: femtosecond laser abaltion in situ SEM, Mater. Charact. 100 (2015) 1–12.